Macromolecular Research, Vol. 17, No. 10, pp 757-762 (2009)

Morphology and Crystallization in Mixtures of Poly(methyl methacrylate)-Poly(pentafluorostyrene)-Poly(methyl methacrylate) Triblock Copolymer and Poly(vinylidene fluoride)

Geon Seok Kim, Min Sung Kang, Mi Ju Choi, Yong Ku Kwon, and Kwang Hee Lee*

Department of Polymer Science and Engineering, Inha University, Incheon 402-751, Korea

Received December 26, 2008; Revised February 27, 2009; Accepted February 27, 2009

Abstract: The microdomain structures and crystallization behavior of the binary blends of poly(methyl methacrylate)-*b*-poly(pentafluorostyrene)-*b*-poly(methyl methacrylate) (PMMA-PPFS-PMMA) triblock copolymer with a low molecular weight poly(vinylidene fluoride) (PVDF) were investigated by small-angle X-ray scattering (SAXS), small-angle light scattering (SALS), transmission electron microscopy (TEM), optical microscopy, and differential scanning calorimetry (DSC). A symmetric, PMMA-PPFS-PMMA triblock copolymer with a PPFS weight fraction of 33% was blended with PVDF in *N,N*-dimethylacetamide (DMAc). In the wide range of PVDF concentration between 10.0 and 30.0 wt%, PVDF was completely incorporated within the PMMA microdomains of PMMA-PPFS-PMMA without further phase separation on a micrometer scale. The addition of PVDF altered the phase morphology of PMMA-PPFS-PMMA from well-defined lamellar to disordered. The crystallization of PVDF significantly disturbed the domain structure of PMMA-PPFS-PMMA in the blends, resulting in a poorly-ordered morphology. PVDF displayed unique crystallization behavior as a result of the space constraints imposed by the domain structure of PMMA-PPFS-PMMA. The pre-existing microdomain structures restricted the lamellar orientation and favored a random arrangement of lamellar crystallites.

Keywords: triblock copolymer, blend, microdomain structure, crystallization.

Introduction

In recent years, many studies have been carried out to determine the morphology of binary mixtures of a block copolymer with a homopolymer.[1-25] The addition of a homopolymer to a block copolymer can cause changes in the microdomain structures and properties of the block copolymer. However, the choice of miscible homopolymers for mixing with block copolymers is limited on account of the poor miscibility of most polymer pairs. Most studies have employed homopolymers with repeat units identical to one of the component blocks of the block copolymers.[1-19] Only a few studies have considered mixtures where the homopolymer is different from either the block segments of the block copolymer, but is miscible with one of the component blocks.[20-25]

In an attempt to investigate the effect of the addition of a semicrystalline homopolymer on the phase-separated morphology of a block copolymer in the mixtures, the present study prepares a series of binary mixtures of an fully-amorphous, symmetric triblock copolymer of poly(methyl methacrylate)-*b*-poly(pentafluorostyrene)-*b*-poly(methyl methacrylate) (denoted as PMMA-PPFS-PMMA) and a semicrystalline homopolymer of poly(vinylidene fluoride) (PVDF). The PVDF molecules have an exothermic interaction with the PMMA blocks through intermolecular hydrogen bonding.[26,27] We also investigate the effect of the confined geometry of the domain structure of PMMA-PPFS-PMMA on the crystallization of PVDF. The complicated morphology could be expected from these blend systems owing to the phase separation in the block copolymer and the crystallization of PVDF. The phase-separated morphology of the domain structure of PMMA-PPFS-PMMA and its blends was monitored by small-angle X-ray scattering (SAXS). The crystallization of PVDF was induced in the blends obtained after cooling from the melts and subsequent annealing at a certain temperature. The melting behavior of the blends was also carefully investigated by using differential scanning calorimetry (DSC).

*Corresponding Author. E-mail: polylee@inha.ac.kr

Experimental

Materials. A symmetric PMMA-PPFS-PMMA with a polydispersity index M_w/M_n=1.23 was synthesized by atom

Table I. Composition of the PVDF/PMMA-PPFS-PMMA Blends

Nomenclature	$W_{(PVDF)}$[a]	$W_{(PVDF+PMMA)}$[b]
B0	0	0.66
B1	0.1	0.70
B2	0.2	0.73
B3	0.3	0.76

[a]Weight fraction of PVDF. [b]Weight fraction of PVDF and PMMA block of the copolymer.

transfer radical polymerization (ATRP). The synthesis and characterization of the PMMA-PPFS-PMMA have been described elsewhere.[28] The M_ns of the PMMA and PPFS blocks were 1.09×10^4 and 1.12×10^4, respectively. A low molecular weight PVDF ($M_n=5.0\times10^3$) was kindly supplied by the Polymer Hybrids Research Center of Korea Institute of Science and Technology. A series of binary mixtures of PVDF and PMMA-PPFS-PMMA were prepared by solution blending method. The predetermined amounts of PVDF and PMMA-PPFS-PMMA were dissolved in *N*,*N*-dimethylacetamide (DMAc) (*ca.* 10 wt% solution). The solvent was evaporated slowly during 1 week at room temperature and further dried for 5 days under vacuum at 60 °C. The microphase-separated domain structure was induced during annealing the cast films of the blends at 180 °C for 3 days under vacuum. The annealed samples were quickly quenched in liquid nitrogen to freeze the morphology at high temperatures. The composition of the blends is listed in Table I.

Transmission Electron Microscopy (TEM). The microphase-separated morphology of the blends was investigated by TEM. The blend films were first embedded with epoxy resin, which were cured at room temperature for additional 12 h. The thin sections of the blend samples with a thickness of approximately 70 nm were obtained by using a Reichert Ultra Microtome, equipped with a diamond knife. The microtomed samples were exposed to RuO_4 (0.5% aqueous solution) for about 10 min for staining the PPFS domain selectively. The TEM data was obtained from a JEOL 1200EX operated at 120 kV.

SAXS. The SAXS experiment was conducted at the synchrotron X-ray beam line 4C1 of the Pohang Light Source (PLS), Korea. The wavelength of the X-ray beam was 0.1608 nm. The distance between the detector and the sample was 170 cm. The scattering intensity (I) was corrected for background scattering. The scattering intensity as a result of thermal fluctuations was then subtracted from the SAXS profile $I(q)$ by evaluating the slope of a $I(q)q^4$ versus q^4 plot at a wide scattering vector q, where q is $(4\pi/\lambda)\sin(\theta/2)$, with λ and θ being the wavelength and scattering angle, respectively. The correction for the smearing effect due to the finite cross section of the incident beam was not necessary for the optics of the SAXS with point focusing.

Optical Microscopy (OM). The miscibility in the melt state and the crystalline morphology of the blends were examined using a Nikon Optiphot 2 microscope equipped with a hot stage. The blend samples were first melted at 180 °C for 10 min, and isothermally crystallized at a crystallization temperature T_c=135 °C. Micrographs of the crystallized samples were taken between crossed polarizers.

Small-Angle Light Scattering (SALS). The supramolecular structures were examined using SALS. The specimen was held at 180 °C for 10 min and then rapidly transferred onto a hot stage set at a crystallization temperature T_c=135 °C in a light scattering apparatus equipped with a charge-coupled device camera. A polarized He-Ne gas laser with 632.8 nm wavelength was applied to the specimen. H_v geometry was employed, where the optical axis of the analyzer was set perpendicular to that of the polarizer.

DSC. Melting thermograms were obtained with a Perkin-Elmer DSC-7 differential scanning calorimetry (DSC). The samples were heated to 200 °C at a rate of 10 °C/min in a nitrogen atmosphere.

Results and Discussion

Morphology. All PVDF/PMMA-PPFS-PMMA blends studied are visually transparent in the melt. The OM observations reveal that the melt morphology of the blends is homogeneous and free of any discernible domains. Considering that the homopolymer has limited solubility in the microdomains of the block copolymer,[4,12,21] the appearance of a homogeneous texture in the wide range of compositions from B1 to B3 (the optical micrographs were omitted) is quite interesting. The miscibility between two polymers may be the result of favorable intermolecular interactions through hydrogen bonding between the carbonyl groups of PMMA of PMMA-PPFS-PMMA and CH_2 units on the PVDF.[26] The relatively low molecular weight of PVDF, compared with that of the PMMA block segment of PMMA-PPFS-PMMA also facilitates the incorporation of PVDF molecules into the PMMA domain of PMMA-PPFS-PMMA. The possible three models are as follows: 1) PVDF is dissolved in the PMMA domain of PMMA-PPFS-PMMA; 2) the part of PVDF is dissolved in the PMMA domain, while the remaining PVDF is located in the center of the microdomain; 3) PVDF is located within the PMMA microdomain, but the PVDF is completely segregated from the PMMA segment, resulting in the formation of a phase-separated morphology that is similar to a core-shell structure. Recently, it was proposed on the basis of the dependence of the lamellar period on the volume fraction of PVDF that the PVDF molecules were located in the middle of the PMMA lamellae.[29]

Figure 1 shows typical transmission electron micrographs obtained from the thin sections of the cast films stained by ruthenium tetraoxide. The dark area in the micrographs represents the PPFS domains, selectively stained by osmium tetraoxide. As shown in Figure 1(a), PMMA-PPFS-PMMA

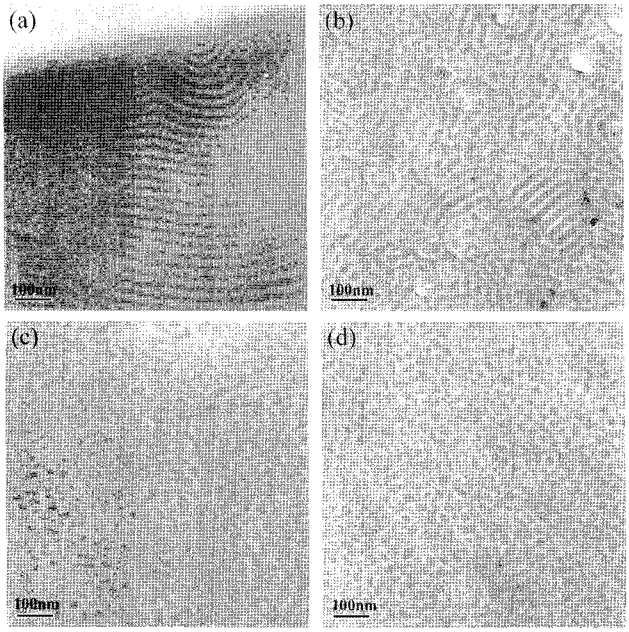

Figure 1. TEM micrographs of the PMMA-PPFS-PMMA and PVDF/PMMA-PPFS-PMMA blends: (a) B0; (b) B1; (c) B2; (d) B3.

exhibits a highly-ordered lamellar morphology with a long-range spatial order. Figure 1(b) shows that the blend B1 prepared by the addition of small amount of PVDF also displays a lamellar morphology. However, the morphology of B1 was much less ordered than that of the neat PMMA-PPFS-PMMA. The order-to-disorder transition becomes clearer with further increasing the concentration of PVDF as seen in Figure 1(c) and (d). In these images, the segregation or rejection of PVDF from the domain structure of PMMA-PPFS-PMMA was not so prominent indicating the successful incorporation of PVDF into the domain structure of PMMA-PPFS-PMMA.

Our SAXS data also provided the evidence for this morphology transition. Figure 2 shows the SAXS scans of $I(q)$ *vs* the scattering vector, q, of the as-cast films of PMMA-PPFS-PMMA and blend samples with various blend compositions. In Figure 2(a), the neat PMMA-PPFS-PMMA (B0) exhibits multiple-order scattering maxima at peak positions (q_m) of 1:2:3, relative to that of the first-order peak (q^*), where q is $(4\pi/\lambda)\sin(\theta/2)$, with λ and θ being the wavelength and scattering angle, respectively. The ratio in the peak position of q_m/q^* suggests that PMMA-PPFS-PMMA is in the lamellar phase.[30] In the SAXS data measured from the B1 sample, as shown in Figure 2(b), we found several Bragg peaks whose q values are almost in the ratio of 1:2:3, indicating that it is also in the lamellar phase. However, these SAXS peaks became more intense than those measured from pure PMMA-PPFS-PMMA. The increase in peak sharpness for the B1 sample may arise from the addition of the low molecular weight PVDF which is in a molten

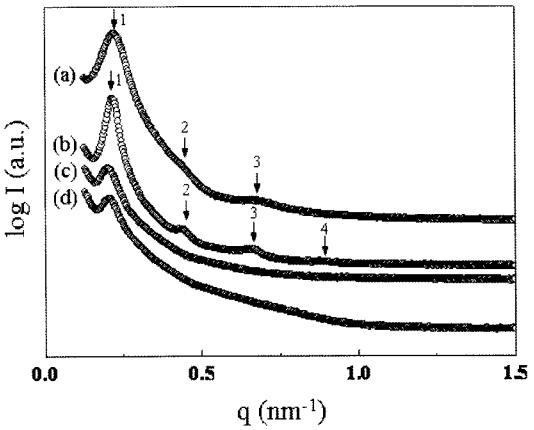

Figure 2. SAXS profiles of the PMMA-PPFS-PMMA and PVDF/PMMA-PPFS-PMMA blends in the melt state: (a) B0; (b) B1; (c) B2; (d) B3.

state during annealing at 180 °C. It may act as a plasticizer for the PMMA microdomain and cause the improvement of the mobility of the PMMA block segments, resulting in the structural reorganization of the microphase-separated domain structure. In addition, the incorporation of PVDF into the PMMA domain enhances the electron contrast with the PPFS domain, which results in an additional increase in the SAXS intensity for the blend systems. As seen in Figure 2(c) and (d), as the PVDF concentration was further increased, the peaks of the SAXS data became broader and weaker, indicating that the domain structure of the blends became disordered. These results suggest that the addition of PVDF causes the morphological changes from an ordered to a disordered domain structure, as demonstrated in the TEM data of Figure 1. It should be noted that the position of the main peak intensity of Figure 1 for the blend samples shifts to a lower $2q$ values, compared with one measured from the PMMA-PPFS-PMMA. The interdomain distances Ds for the B0, B1, B2, and B3 samples were determined from the main peak intensity as 28.0, 28.8, 31.2, and 30.8 nm, respectively. The change in the D values suggests that the interdomain distance might be increased by the structural disorder, occurring due to swelling of the PMMA microdomain due to the incorporation of the PVDF molecules.

In general, polymeric crystals can grow at a long-range order in a micrometer level. For the blends of block copolymers with semicrystalline polymers, the crystallization of semicrystalline polymers may disturb the morphology of block copolymers as given by the volume fraction of component blocks. In particular, it is possible that the microphase morphology of block copolymers is significantly distorted if the crystallization temperature of semicrystalline polymers is higher than the T_g values of the block segments. Figure 3 shows the SAXS patterns for the blends, isothermally crystallized at 135 °C after annealing PMMA-PPFS-PMMA at high temperature into a phase-separated melt state. In Fig-

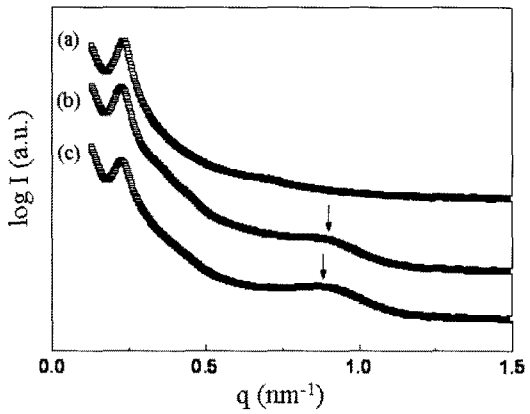

Figure 3. SAXS profiles of the PVDF/PMMA-PPFS-PMMA blends crystallized at 135 °C: (a) B1; (b) B2; (c) B3.

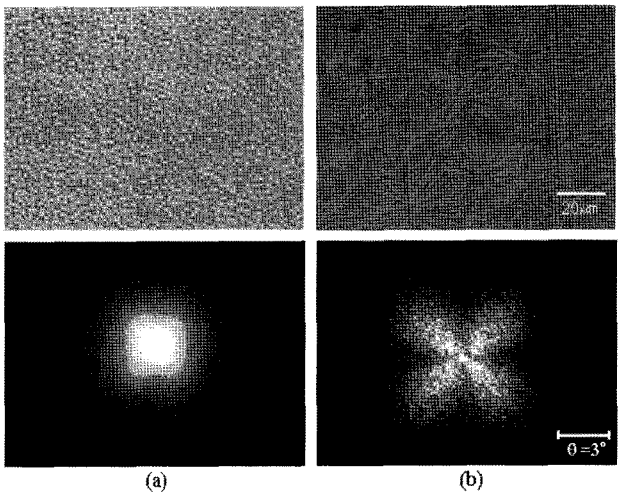

Figure 4. Optical micrographs of the PVDF/PMMA-PPFS-PMMA blends crystallized at 135 °C and the corresponding SALS H_v patterns: (a) B2; (b) B3.

ure 3(a) measured from the B1 blend, the main SAXS peak became much broader without any additional higher peaks, indicating that the domain structure of PMMA-PPFS-PMMA was severely disturbed due to the crystallization of PVDF. The PPFS and PMMA blocks are in a rubbery phase at the crystallization temperature (135 °C) of PVDF. Therefore, it is likely that the crystal front of PVDF, grown at a long-range order, disturbs the structural perfection of the pre-formed domain structure of PMMA-PPFS-PMMA. One of the interesting features in this figure is the change in the long period, L, of the PVDF crystals (the q value corresponding to L is denoted as an arrow in the figure). The L values of B2 and B3 are 71.3 and 72.6 Å, respectively, which are smaller than the L value of 80.2 Å for the homo-PVDF (SAXS pattern for the homo-PVDF is not given). The considerable decrease of the long period implies that the lamellar dimensions of PVDF such as the crystal thickness and amorphous layer thickness might also be influenced by the pre-existing microdomain structures.

Crystallization. The crystallization behavior of the blends appears to be significantly different from that of homo-PVDF, because the microdomain structure of PMMA-PPFS-PMMA in the melt state provides spatial, nanoscale constraints to the crystal growth of PVDF and thereby retards the crystal growth of PVDF as an additive homopolymer.[31,32] The confined crystallization in an ordered phase morphology can be largely changed depending on the relative location of the crystallization temperature (T_c) and the glass transition temperature of the block segments (T_g), as relative to the order-disorder transition temperature of the block copolymer (T_{ODT}). In the case of $T_c < T_g < T_{ODT}$, the crystallization of a homopolymer is strongly confined by the glassy blocks within the pre-existing phase morphology. This is known as hard confinement. On the other hand, in the case of $T_g < T_c < T_{ODT}$, a homopolymer may have more freedom for crystallization within the relatively-soft pre-existing phase morphology (soft confinement). In case of the blend of PMMA-PPFS-PMMA with PVDF, as described in the previous section, both PPFS and PMMA blocks are in a rubbery state at the crystallization temperature (135 °C) of PVDF, and therefore the domain structure of the blends was highly distorted by the crystallization of PVDF.

Figure 4 shows optical micrographs with crossed polarizers and the corresponding SALS H_v patterns for B2 and B3 blends isothermally crystallized at 135 °C after annealing PMMA-PPFS-PMMA at high temperature into a phase-separated melt state. In the case of the B1 blend, the OM image and SALS pattern could not be obtained because of the relatively low crystallinity. A typical spherulitic structure, which is similar in appearance to a 'Maltese Cross' extinction pattern, is not observed in any of the samples. This indicates that the pre-existing microdomain structures restrict the lamellar orientations and favor the random arrangement of individual lamellar crystallites. It is worth noting that the SALS patterns provide a direct evidence of the evolution of a spherulitic superstructure, even though the formation of spherulites is not observed optically. In Figure 4(a), the B2 blend shows a diffuse and less azimuthally dependent scattering pattern. The H_v scattering pattern is related to the large-scale arrangement of the individual lamellar crystallites. Stein and Chu[33] reported that lower order of organization results in a broad H_v scattering pattern. As the degree of disorder of the lamellar orientation increases, the azimuthal dependence of the scattering pattern is reduced and the scattering pattern shows a diffuse pattern. In the case of B2 blend with a lamellar morphology, the crystal orientation of PVDF may be dependent on the contour of the PMMA/PVDF domain boundary. In Figure 4(a), the diffuse H_v pattern of the B2 blend strongly suggests that the crystal growth path is highly distorted, because the crystals are confined such that they can only grow within the microsepa-

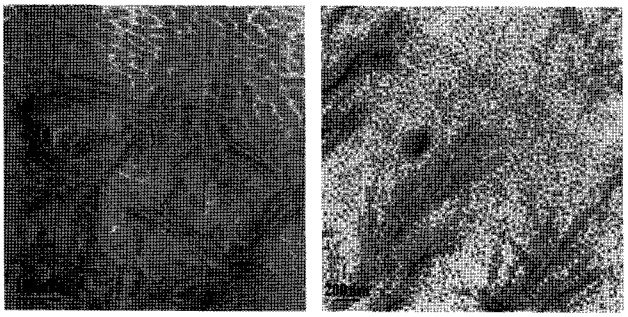

Figure 5. TEM micrographs of the PVDF/PMMA-PPFS-PMMA blends crystallized at 135 °C: (a) B2; (b) B3.

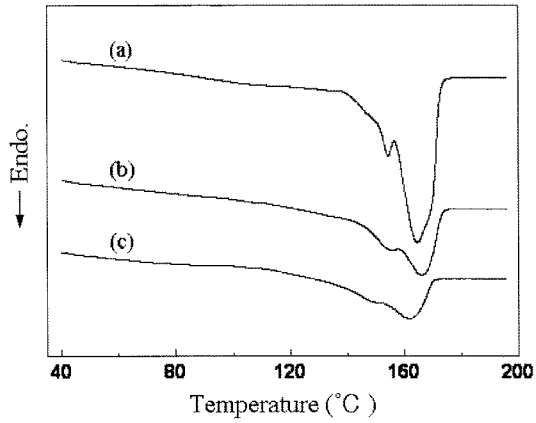

Figure 6. Melting endotherms of the homo-PVDF and PVDF/PMMA-PPFS-PMMA blends: (a) homo-PVDF; (b) B2; (c) B3. The heating rate was 10 °C/min.

rated domains. On the other hand, as shown in Figure 4(b), the B3 blend exhibits a four-leaf clover pattern, which is representative of a high order of organization within the spherulites.[33] As seen in Figure 1(d), B3 blend contains a randomly dispersed, isolated PPFS phase with the surrounding matrix, composed exclusively of the PMMA and PVDF constituents. Therefore, the observation of a four-leaf clover pattern in the B3 blend suggests that the tendency of the crystal growth of PVDF will be undisturbed within the majority matrix phase.

Figure 5 shows the TEM images of the blends crystallized at 135 °C: (a) B2; (b) B3. These data provide supplementary evidence for the organization of the PVDF lamellar crystals in the blends. In Figure 5(a), the crystalline PVDF lamellae, appeared as stripes, are arranged multidirectionally and are curved in the B2 blend, whereas the radiating PVDF lamellae are arranged with a relatively high degree of orientational correlation of the constituent crystals in Figure 5(b) for B3. These results are consistent with the results measured from the light scattering experiment: a rodlike scattering and a four-leaf clover pattern for B2 and B3, respectively.

The effects of the confined crystallization on the melting behavior of PVDF are evaluated. Figure 6 shows the DSC thermograms for the blend samples isothermally crystallized at 135 °C after annealing PMMA-PPFS-PMMA at high temperature into a phase-separated melt state. It is well known that PVDF has multiphase characteristics with four widely accepted crystalline forms (α, β, γ, and δ phases).[34] The β-phase, with an almost planar zigzag conformation, has the highest piezoelectric constant, whereas the α-phase, with a TGTG' conformation, is electrically inactive, because the molecular dipoles in the unit cell negate each other. Considering that the melting temperatures of the α- and β-phase of the PVDF crystal forms are similar, this multiple melting behavior may be associated with melting, recrystallization, and remelting process of PVDF crystals in the melting region. It is interesting to describe that a higher melting endotherm was observed for B2 in Figure 6(b). The melting temperature (T_m) can be expressed as a ratio of the change in the enthalpy (ΔH_m) and entropy (ΔS_m) during melting ($T_m = \Delta H_m/\Delta S_m$). ΔH_m is a term that is determined by the interaction between the molecular chains, and is almost constant if the crystalline structure is similar. One the other hand, ΔS_m depends on the chain conformations of the melt and crystalline state, and is mainly controlled by the freedom of the chain conformation in the melt state. For B2, PVDF is spatially confined within the PMMA lamellar microdomain in a nanometer level. The confined PVDF chains have a relatively lower degree of freedom in the conformation than those located in a free space. As a result, ΔS_m of the confined chains is smaller than that of the free chains. Because T_m is given by $\Delta H_m/\Delta S_m$, a smaller ΔS_m means a higher T_m. Based on this consideration, the higher melting endotherm for B2 appears due to the decrease in ΔS_m as a result of the chain confinement within the domain structure. It is also interesting that the position of the endothermic peaks slightly shifts to low temperatures for B3. This result may be due to the disordered domain structure of B3 which fails to restrict the PVDF crystals within the lamellar domain structure of PMMA-PPFS-PMMA. Because B3 blend contains a continuous matrix phase, composed of the PMMA and PVDF constituents, it is likely that the PVDF chains have a higher degree of freedom in the conformation and their ΔS_m in the case of B3 is larger than those of the restricted chains, leading to lower melting points for B3.

Conclusions

This study examined the morphological changes and crystallization behavior of PVDF/PMMA-PPFS-PMMA blends. The addition of PVDF in the domain structure of PMMA-PPFS-PMMA changed the morphology from an ordered to a disordered domain structure. The crystallization of PVDF caused a rearrangement and/or disturbance of the microdomain structure, resulting in a decrease in the structural

order of the blends. PVDF exhibited unique crystallization behavior depending on space constraints. The crystal growth pattern was highly dependent on the pre-existing microdomain structures, because the confined crystallization proceeded within the ordered-phase morphology.

Acknowledgements. This research was supported by an Inha University Research Grant. Synchrotron SAXS experiments were performed at the Pohang Light Source (4C1 beam line) in Korea.

References

(1) T. Hashimoto, H. Tanaka, and H. Hasegawa, *Macromolecules*, **23**, 4378 (1990).
(2) H. Tanaka, H. Hasegawa, and T. Hashimoto, *Macromolecules*, **24**, 240 (1991).
(3) K. I. Winey, E. L. Thomas, and L. J. Fetters, *Macromolecules*, **24**, 6182 (1991).
(4) R. J. Roe and W. C. Zin, *Macromolecules*, **17**, 189 (1984).
(5) C. Prahsarn and M. Jamieson, *Polymer*, **38**, 1273 (1997).
(6) D. J. Meier, *Polym. Prepr.* (Am. Chem. Soc., Div. Polym. Chem.), **18**, 340 (1977).
(7) L. Z. Liu, F. Yeh, and B. Chu, *Macromolecules*, **29**, 5336 (1996).
(8) L. Z. Liu, H. Li, B. Jiang, and E. Zhou, *Polymer*, **35**, 5511 (1994).
(9) H. K. Lee, C. K. Kang, and W. C. Zin, *Polymer*, **37**, 287 (1996).
(10) L. Z. Liu and B. Chu, *J. Polym. Sci. Part B: Polym. Phys.*, **37**, 779 (1999).
(11) K. Sakurai, W. J. Macknight, D. J. Lohse, D. N. Schuiz, J. A. Sissano, J. S. Lin, and M. Agamalyan, *Polymer*, **37**, 4443 (1996).
(12) K. Sakurai, W. J. Macknight, D. J. Lohse, D. N. Schulz, and J. A. Sissano, *Macromolecules*, **27**, 4941 (1994).
(13) K. Sakurai, W. J. Macknight, D. J. Lohse, D. N. Schulz, and J. A. Sissano, *Macromolecules*, **26**, 3236 (1993).
(14) L. Zhu, B. R. Mimnaugh, Q. Ge, R. P. Quirk, S. Z. D. Cheng, E. L.Thomas, B. Lotz, B. S. Hsio, F. Yeh, and L. Liu, *Polymer*, **42**, 9121 (2001).
(15) P. Rangarajan, C. F. Haisch, R. A. Register, D. H. Adamson, and L. J. Fetters, *Macromolecules*, **30**, 494 (1997).
(16) A. Buzarovska, S. Koseva, M. Cvetkovska, and E. Nedkov, *Eur. Polym. J.*, **37**, 141 (2001).
(17) G. Radonjic and I. Smit, *J. Polym. Sci. Part B: Polym. Phys.*, **39**, 566 (2001).
(18) W. Lee, H. L. Chen, and T. L. Lin, *J. Polym. Sci. Part B: Polym. Phys.*, **40**, 519 (2002).
(19) B. Lowenhaupt and G. P. Hellmann, *Polymer*, **32**, 1065 (1991).
(20) T. Hashimoto, K. Kimishima, and H. Hasegawa, *Macromolecules*, **24**, 5704 (1991).
(21) X. Lu and R. A. Weiss, *Macromolecules*, **26**, 3615 (1993).
(22) M. C. Luyten, E. J. F. Bogels, G. O. R. Alberba van Ekenstein, G. ten Brinke, W. Bras, B. E. Komanschek, and A. J. Ryan, *Polymer*, **38**, 509 (1997).
(23) J. K. Kim, D. S. Jung, and J. H. Kim, *Polymer*, **34**, 4613 (1993).
(24) H. Zhao, L. Liu, T. Tang, and B. Huang, *Polym. J.*, **30**, 775 (1998).
(25) H. K. Lee, C. K. Kang, and W. C. Zin, *Polymer*, **38**, 1595 (1997).
(26) T. Nishi and T. T. Wang, *Macromolecules*, **8**, 909 (1975).
(27) B. S. Morra and R. S. Stein, *J. Polym. Sci., Polym. Phys. Ed.*, **20**, 2243 (1982).
(28) Y. S. Ko, J. H. Oh, K. B. Kim, H. S. Park, M. S. Kim, and Y. K. Kwon, *Macromol. Res.*, **17**, 623 (2009).
(29) S. I.Yoo, S. H. Yun, J. M. Choi, B. H. Shon, W. C. Zin, J. C. Jung, K. H. Lee, S. M. Jo, J. Cho, and C. Park, *Polymer*, **46**, 3776 (2005).
(30) I. W. Hamley, *The Physics of Block Copolymers*, Oxford Science Publications, New York, 1998.
(31) H. L. Chen, S. C. Hasiao, T. L. Lin, K. Yamauchi, H. Hasegawa, and T. Hashimoto, *Macromolecules*, **34**, 671 (2001).
(32) H. L. Chen, J. C. Wu, T. L. Lin, and J. S. Lin, *Macromolecules*, **34**, 6936 (2001).
(33) R. S. Stein and W. Chu, *J. Polym. Sci. A-2*, **8**, 1137 (1970).
(34) J. B. Lando, H. G. Olf, and A. Peterlin, *J. Polym. Sci. A-1*, **4**, 941 (1966).